La Société Savante de l'Aéronautique et de l'Espace

53rd 3AF International Conference on Applied Aerodynamics
26 – 28 March 2018, Salon de Provence – France

FP26-AERO2018-kirsch

Computation of very flexible high-aspect-ratio composite wing flutter speed using optimised open source solver

Bertrand Kirsch[(1)], Olivier Montagnier[(1)], Emmanuel Bénard[(2)], Thierry M. Faure[(1)]
[(1)]Centre de Recherche de l'Armée de l'air, École de de l'Air, 13661 Salon Air, France
bertrand.kirsch@defense.gouv.fr, olivier.montagnier@defense.gouv.fr, thierry.faure@defense.gouv.fr
[(2)]Département Conception et conduite des véhicules Aéronautiques et Spatiaux (DCAS)
Institut Supérieur de l'Aéronautique et de l'Espace Supaéro
10 avenue Édouard-Belin, BP 54032 - 31055 Toulouse CEDEX 4, emmanuel.benard@isae.fr

ABSTRACT

The enhancement of high altitude drone endurance compels to design very flexible high aspect ratio composite airframe vulnerable to destructive fluid/structure interaction like flutter or torsional divergence. Aeroelastic tailoring, a specific configuration of laminated composite layup, appears to be a promising way to increase critical speed without being at the expense of weight balance. The present work presents an aeroelastic reduced order model suitable for the non linear anisotropic behavior of this kind of composite wing and able to quickly compute critical speed like flutter with the intent of using it in an optimisation loop. In this regard, particular attention is devoted to computational efficiency using optimised open source solver like MUMPS and ARPACK.

1 INTRODUCTION

Recent progress made in the field of solar cells, energy storage and composite materials pave the way to a new concept of aircraft, namely High Altitude Pseudo Satellites (HAPS). Among them, a particular type of solar or/and hydrogen powered High Altitude Long Endurance (HALE) Unmanned Aerial Vehicles (UAV) aims to meet a virtually infinite endurance. To achieve this far-reaching goal, because of the low on-board power, aerodynamic and structural performances are stretched to their limits. This results, on the aerodynamic side, in high-aspect ratio wing optimising the lift-to-drag ratio and, on the structural side, in lightweight very flexible composite airframe. The main drawback of this particular design is its vulnerability to destructive fluid/structure interactions like torsional divergence and flutter. Classical solutions designed to further aeroelastic critical speed mostly rely on the stiffening of the airframe or the adjustment of mass distribution. Both options are detrimental to mass balance which is a key feature of HAPS. In that context, alternative solutions should be explored, among these are aeroelastic tailoring discussed below.

The nature of a fluid/structure interaction strongly depends on the system characteristics. Different approximations are made depending on the motion of structure relatively to the fluid. In order to quantify that, dimensionless numbers are used. In our case, the degree of fluid/structure coupling is characterised by the reduced frequency $f_r = T_f/T_s$ with T_f the period of fluid motion and T_s the period of structure motion. Solar powered HALE UAV, because of their large wingspan and their low flight speed (for instance 75 m wingspan and 35 km/h for NASA Helios UAV), are characterised by a reduced frequency near 1. In fact, it means that both dynamic are tightly linked. Therefore, high fidelity simulation of this kind of fluid structure/interaction with a finite volume method coupled with a finite element method still leads to a prohibitive computational cost. Indeed, it implies an unsteady resolution with a very small time step of both problem (fluid and structure) and the transfer between fluid and solid of position and velocity informations. Consequently, aeroelastic reduced order model are still widely used, especially for Very Flexible Aircraft (VFA). The large displacement and rotation encountered by a very flexible wing associated with a low flight speed make the aeroelastic behavior all the more difficult

to simulate because of the induced geometrical non linearities and the fluid motion instationarities.

A relevant illustration of the need for an accurate modelling of theses phenomena is the accident of the Helios UAV which occurred on the 26th June 2003 due to a large deflection and rotation of the wing leading to an unstable pitch oscillation [1]. To meet this need, several reduced order aeroelastic model have been developed. For computational efficiency, most of them are based on inviscid, incompressible potential flow theory coupled with beam or plate theories. We could mention computation code NANSI (Nonlinear-Aerodynamics/ Nonlinear-Structure Interaction) [2] which combines an Unsteady Vortex Lattice Method (UVLM) and a nonlinear beam theory. The UVLM is particularly useful in case of low-aspect-ratio wing or delta wing because the method is able to predict 3D effects. Another solution is proposed by Murua in SHARP program (Simulation of High Aspect Ratio Planes) [3] using UVLM with a displacement based geometrically exact beam theory. Some models are dedicated to high-aspect-ratio wing like Drela's program ASWING [4]. This VFA conception tool combines a nonlinear isotropic beam formulation with an unsteady lifting line theory. More recently, Shearer and Cesnik have developed a Matlab toolbox called UM/NAST (University of Michigan/ Nonlinear Aeroelastic Simulation Toolbox) [5] made up of a strain-based geometrically nonlinear beam formulation linked with a finite state two-dimensional incompressible flow aerodynamic theory proposed by Peters and al [6]. A similar formulation is used by Ribeiro in the Matlab toolbox Aeroflex [7].

Because aeroelastic tailoring exploits the anisotropy of composite materials, a suited reduced order model must take this anisotropy into account. This capability resides in the Matlab toolbox proposed by Patil and Hodges called NATASHA (Nonlinear Aeroelastic Trim and Stability of HALE Aircraft) [8] coupling an intrinsic beam formulation with Peters' theory.

The present paper presents an efficient open source implementation of an aeroelastic reduced order model coupling a nonlinear anisotropic beam theory with unsteady two-dimensional aerodynamic Peters' model. Computation speed and accuracy of this implementation is then assessed using widely used aeroelastic test cases.

2 AEROELASTIC REDUCED ORDER MODEL

The high aspect ratio assumption gives us the opportunity to neglect tridimensional effects and thus to use a strip theory which can be easily linked to a beam formulation.

This implementation can be done in two different ways:

- A loose coupling consisting in defining the aerodynamic loads to apply on the beam in accordance with position and speed parameters extracted from the last structural calculation. This method is easy to implement and is well suited for modular architecture like, for instance, the wind turbines conception software FAST from the NREL [9]. However, it also has its drawbacks like the inability to perform coupled eigenvalue analysis or some convergence issues for nonlinear Newton-Raphson algorithms (aerodynamic loads are not taken into account into the Jacobian matrix). It also implies in our ranges of reduced frequencies a very small time step.

- A tight coupling done by integrating aerodynamic loads directly into the weak formulation of the beam theory. This approach is much more complex and is not really adapted to modular architecture but allows to overcome the main drawbacks of a loose coupling. Indeed, the most interesting application is the possibility to determine, for a particular flow velocity, the aeroelastic modes of the wing about a steady sate, namely frequencies, modal shapes and damping factors. The latter is a key parameter for our study because it defines the limit between stable and unstable speed and thereby provide the flutter boundary. Concomitantly, a zero-frequency mode for a given flow velocity indicates torsional divergence speed overrun.

Consequently, the tight coupling has been chosen for our toolbox.

2.1 Aeroelastic tailoring

Aeroelastic tailoring consists in exploiting laminate composite anisotropy by setting a proper layup. For most applications, a laminate layup presents a mirror symmetry with respect to its middle plane. If we consider a laminate plate of unidirectional (UD) plies, the layup [-45°, 0°, 45°, 90°, 90°, 45°, 0°, -45°], with angular values representing fiber orientation in each ply, presents a mirror symmetry. The aim of this type of symmetry is to dissociate membrane behavior (inplane loadings imply inplane displacements and vice versa) from bending behavior. It is especially useful to avoid the warping of a hot polymerised laminate plate during cool down. Another common rule concerning the UD plies orientation is to set balanced layup, namely to put for instance as many -45° plies as 45° plies. It is meant to avoid coupling between the different bending behavior. The true principle of aeroelastic tailoring is to ignore these rules, thus allowing coupling between the different behaviors of the laminate. It mainly consists in creating a link between the bending and the warping of the laminate. On the aerodynamic side, it induces the coupling of the bending due to lift forces and the twisting of the wing which determines the local Angle of Attack (AoA). Thus, the aeroelastic

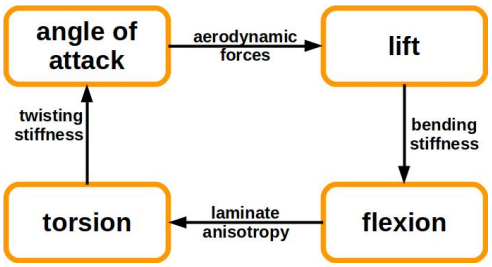

Figure 1: Principle of feedback loop induced by aeroelastic tailoring

tailoring is a way of establishing a feedback loop on the aeroelastic behavior of a very flexible aircraft (figure 1).

2.2 Geometrically exact beam theory

In that context, it is essential to ensure a proper modelling of the laminate anisotropy and geometrical non linearity. For this purpose, the choice fell on an open source tool named GEBT (Geometrically Exact Beam Theory) developed by Yu and Blair [10] designed for composite slender structures under large deflections and rotations, assuming the strains to be small. This tool coded in Fortran 90/95 implements a mixed variational formulation based on exact intrinsic equations for dynamics of moving beams developed by Hodges [11].

The exact intrinsic equations for dynamics are derived from Hamilton's weak principle asymptotically developed along the beam axes:

$$\int_{t_1}^{t_2}\int_0^L \left[\delta\left(K-U\right)+\overline{\delta W}\right] dx_1 dt \quad = \quad \overline{\delta A} \qquad (1)$$

where t_1 and t_2 are arbitrary fixed times, K and U are the kinetic and strain internal energy, respectively, δ is the usual Lagrangian variation for a fixed time, $\overline{\delta W}$ is the virtual work of applied loads and $\overline{\delta A}$ the virtual action on the same period. The resulting formulation is detailed in Hodges [11].

The main strength of this method compared to classical displacement based formulation is to avoid the dependency from a coordinate system (intrinsic nature) for the position and rotation parameters. Kinematical and constitutive relations are then added to the weak formulation with Lagrange multipliers (mixed nature). The resulting formulation allow a finite element implementation with very simple shape functions (constant or linear). According to Hodges [12], we defined three coordinates systems (figure 2):

- a unique global body attached frame a $(\vec{x}_a,\vec{y}_a,\vec{z}_a)$ moving with a given linear and angular velocity $\vec{v}_a$ and $\vec{\omega}_a$ in an inertial frame and consistent with flight mechanics conventions ($\vec{x}_a$ pointing towards, $\vec{y}_a$ pointing the right wing and $\vec{z}_a$ pointing downwards).

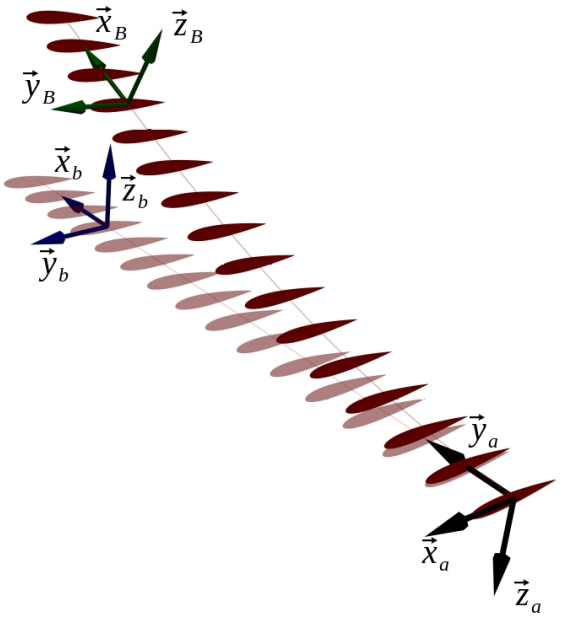

Figure 2: structural frames definition

- at least one undeformed beam frame b $(\vec{x}_b,\vec{y}_b,\vec{z}_b)$ fixed in frame a: $\vec{x}_b$ is tangent to the reference line of the undeformed beam. In our case, a frame b is defined for each section of the wing with a different dihedral or/and wing-sweep.
- a deformed beam frame B $(\vec{x}_B,\vec{y}_B,\vec{z}_B)$ for each beam element: $\vec{x}_B$ is tangent to the deformed beam reference line and points to the right, $\vec{y}_B$ has a chordwise direction and points the upstream flow and $\vec{z}_B$ completes the triad.

Direction cosine matrix describing the rotation between frames are defined using Rodrigues parameters $\theta_i = 2e_i\tan(\alpha/2)$ with α the magnitude of the rotation about a unit vector $\vec{e}$:

$$\vec{\vec{C}} = \frac{\left[1-(1/4)\vec{\theta}^T\vec{\theta}\right]\vec{\vec{\Delta}}-\tilde{\theta}+(1/2)\vec{\theta}^T\vec{\theta}}{1+(1/4)\vec{\theta}^T\vec{\theta}} \qquad (2)$$

with $\vec{\vec{\Delta}}$ the identity matrix and the tilde notation defining a matrix using the following identity for any vector $\vec{w}$:

$$\tilde{\theta}\vec{w} = \vec{\theta}\wedge\vec{w} \qquad (3)$$

Fundamentals unknowns of this formulation are the displacement $\vec{u}_a$ and the Rodrigues parameters $\vec{\theta}_a$ in frame a, the internal forces and moments $\vec{F}_B$ and $\vec{M}_B$ in frame B and the linear and angular momenta $\vec{P}_B$ and $\vec{H}_B$ in frame B. These unknowns are linked to the weak formulation with the following expressions:

$$\left\{\begin{array}{c}\vec{P}_B\\ \vec{H}_B\end{array}\right\} = \left\{\begin{array}{c}\frac{\partial K}{\partial \vec{V}_B}\\ \frac{\partial K}{\partial \vec{\Omega}_B}\end{array}\right\} = \vec{\vec{I}}\left\{\begin{array}{c}\vec{V}_B\\ \vec{\Omega}_B\end{array}\right\} \qquad (4)$$

$$\left\{ \begin{array}{c} \vec{F}_B \\ \vec{M}_B \end{array} \right\} = \left\{ \begin{array}{c} \frac{\partial U}{\partial \vec{V}_B} \\ \frac{\partial U}{\partial \vec{\Omega}_B} \end{array} \right\} = \vec{\vec{S}} \left\{ \begin{array}{c} \vec{\gamma} \\ \vec{\kappa} \end{array} \right\} \tag{5}$$

with $\vec{V}_B$ and $\vec{\Omega}_B$ the linear and angular velocity in the inertial frame developed in frame B, $\vec{\gamma}$ and $\vec{\kappa}$ the strains and curvatures developed in frame B, $\vec{\vec{I}}$ is the mass matrix and $\vec{\vec{S}}$ the stiffness matrix.

The anisotropic nature of the beam is concentrated in Eq. (5). $\vec{\vec{I}}$ and $\vec{\vec{S}}$ matrix are the cross sectional properties of the beam and could be determined by various means. Proprietary program VABS [13] is used in [10]. The present work uses a 3D finite element reduction done with the open source solver Calculix [14] detailed in [15]. Eqs (4)-(5) are expanded below in frame B:

$$\left\{ \begin{array}{c} \gamma_{11} \\ 2\gamma_{12} \\ 2\gamma_{13} \\ \kappa_1 \\ \kappa_2 \\ \kappa_3 \end{array} \right\} = \left[\begin{array}{cccccc} S_{11} & S_{12} & S_{13} & S_{14} & S_{15} & S_{16} \\ S_{12} & S_{22} & S_{23} & S_{24} & S_{25} & S_{26} \\ S_{13} & S_{23} & S_{33} & S_{34} & S_{35} & S_{36} \\ S_{14} & S_{24} & S_{34} & S_{44} & S_{45} & S_{46} \\ S_{15} & S_{25} & S_{35} & S_{45} & S_{55} & S_{56} \\ S_{16} & S_{26} & S_{36} & S_{46} & S_{56} & S_{66} \end{array} \right] \left\{ \begin{array}{c} F_1 \\ F_2 \\ F_3 \\ M_1 \\ M_2 \\ M_3 \end{array} \right\} \tag{6}$$

$$\left\{ \begin{array}{c} P_1 \\ P_2 \\ P_3 \\ H_1 \\ H_2 \\ H_3 \end{array} \right\} = \left[\begin{array}{cccccc} \mu & 0 & 0 & 0 & \mu x_{m3} & -\mu x_{m2} \\ 0 & \mu & 0 & -\mu x_{m3} & 0 & 0 \\ 0 & 0 & \mu & \mu x_{m2} & 0 & 0 \\ 0 & -\mu x_{m3} & \mu x_{m2} & i_{22}+i_{33} & 0 & 0 \\ \mu x_{m3} & 0 & 0 & 0 & i_{22} & -i_{23} \\ -\mu x_{m2} & 0 & 0 & 0 & -i_{23} & i_{33} \end{array} \right] \left\{ \begin{array}{c} V_1 \\ V_2 \\ V_3 \\ \Omega_1 \\ \Omega_2 \\ \Omega_3 \end{array} \right\} \tag{7}$$

with S_{ij} the coefficients of the flexibility matrix, μ the mass per unit length, x_{m2}, x_{m3} the coordinates of the mass center about respectively $\vec{y}_B$ and $\vec{z}_B$, i_{22} the mass moment of inertia about $\vec{y}_B$, i_{33} the mass moment of inertia about $\vec{z}_B$ and i_{23} the product of inertia.

Dividing a beam into N elements with the starting node of the ith element numbered as i and the ending node numbered as $i+1$ and using linear or constant shape function for the unknowns, the initial weak formulation leads to:

$$\begin{aligned} &\sum_{i=1}^{N} \Big\{ \delta\vec{u}_i^T \vec{f}_{u_i}^- + \delta\vec{u}_{i+1}^T \vec{f}_{u_i}^+ + \overline{\delta\vec{\psi}_i^T} \vec{f}_{\psi_i}^- + \overline{\delta\vec{\psi}_{i+1}^T} \vec{f}_{\psi_i}^+ + \overline{\delta\vec{F}_i^T} \vec{f}_{F_i}^- + \\ &+ \overline{\delta\vec{F}_{i+1}^T} \vec{f}_{F_i}^+ + \overline{\delta\vec{M}_i^T} f_{M_i}^- + \overline{\delta\vec{M}_{i+1}^T} \vec{f}_{M_i}^+ + \overline{\delta\vec{P}_i^T} \vec{f}_{P_i} + \overline{\delta\vec{H}_i^T} \vec{f}_{H_i} \Big\} \\ &= \delta\vec{u}_{N+1}^T \hat{\vec{F}}_{N+1} + \overline{\delta\vec{\psi}_{N+1}^T} \hat{\vec{M}}_{N+1} - \overline{\delta\vec{F}_{N+1}^T} \hat{\vec{u}}_{N+1} - \overline{\delta\vec{F}_{N+1}^T} \hat{\vec{\theta}}_{N+1} \\ &- \overline{\delta\vec{F}_{N+1}^T} \hat{\vec{u}}_{N+1} - \delta\vec{u}_1^T \hat{\vec{F}}_1 - \delta\vec{\psi}_1^T \hat{\vec{M}}_1 + \delta\vec{F}_1^T \hat{\vec{u}}_1 + \delta\vec{M}_1^T \hat{\vec{\theta}}_1 \end{aligned} \tag{8}$$

with $\delta\vec{u}$ the virtual displacement, $\delta\vec{\psi}$ the virtual rotation, $\hat{()}$ the boundary conditions and:

$$\begin{aligned} \vec{f}_{u_i}^{\pm} = \quad & \pm\vec{\vec{C}}^T \vec{\vec{C}}^{ab} \vec{F}_i - \overline{\vec{f}_i}^{\pm} \\ & + \tfrac{\Delta L_i}{2} \left[\tilde{\omega}_a \vec{\vec{C}}^T \vec{\vec{C}}^{ab} \vec{P}_i + \overline{\dot{\vec{\vec{C}}}^T \vec{\vec{C}}^{ab}} \vec{P}_i \right] \end{aligned} \tag{9}$$

$$\begin{aligned} \vec{f}_{\psi_i}^{\pm} = \quad & \pm\vec{\vec{C}}^T \vec{\vec{C}}^{ab} \vec{M}_i - \overline{\vec{m}_i}^{\pm} + \tfrac{\Delta L_i}{2} \Big[\tilde{\omega}_a \vec{\vec{C}}^T \vec{\vec{C}}^{ab} \vec{H}_i \\ & + \overline{\dot{\vec{\vec{C}}}^T \vec{\vec{C}}^{ab}} \vec{H}_i + \vec{\vec{C}}^T \vec{\vec{C}}^{ab} \left(\tilde{V}_i \vec{P}_i - (\tilde{e_1} + \tilde{\gamma}_i) \vec{F}_i \right) \Big] \end{aligned} \tag{10}$$

$$\vec{f}_{F_i}^{\pm} = \pm\vec{u}_i - \frac{\Delta L_i}{2} \left[\vec{\vec{C}}^T \vec{\vec{C}}^{ab} (\vec{e}_1 + \vec{\gamma}_i) - \vec{\vec{C}}^{ab} \vec{e}_1 \right] \tag{11}$$

$$\vec{f}_{M_i}^{\pm} = \pm\vec{\theta}_i - \frac{\Delta L_i}{2} \left(\vec{\vec{\Delta}} + \frac{\tilde{\theta}}{2} + \frac{\vec{\theta}_i \vec{\theta}_i^T}{4} \right) \vec{\vec{C}}^{ab} \vec{\kappa}_i \tag{12}$$

$$\vec{f}_{P_i} = \vec{\vec{C}}^T \vec{\vec{C}}^{ab} \vec{V}_i - \vec{v}_i - \tilde{\omega}_a \vec{u}_i - \dot{\vec{u}}_i \tag{13}$$

$$\vec{f}_{H_i} = \vec{\Omega}_i - \vec{\vec{C}}^{ba} \vec{\vec{C}} \vec{\omega}_a - \vec{\vec{C}}^{ba} \frac{\vec{\vec{\Delta}} - \tilde{\theta}_i/2}{1 + \vec{\theta}_i \vec{\theta}_i^T/4} \dot{\vec{\theta}}_i \tag{14}$$

with $\vec{e}_1 = \begin{pmatrix} 1 & 0 & 0 \end{pmatrix}^T$, $\vec{\vec{C}}$ the matrix direction cosines between frame b and B, $\vec{\vec{C}}^{ab}$ the matrix direction cosines between frame b and a, $\vec{\vec{C}}^{ba} = \left(\vec{\vec{C}}^{ba} \right)^T$, ΔL_i the length of the ith element and $\overline{\vec{f}_i}^{\pm}$, $\overline{\vec{m}_i}^{\pm}$ the discretised distributed forces and moments defined by:

$$\overline{\vec{f}_i}^{-} = \int_0^1 (1-\xi) \vec{f}_a \Delta L_i d\xi; \quad \overline{\vec{f}_i}^{+} = \int_0^1 \xi \vec{f}_a \Delta L_i d\xi \tag{15}$$

$$\overline{\vec{m}_i}^{-} = \int_0^1 (1-\xi) \vec{m}_a \Delta L_i d\xi; \quad \overline{\vec{m}_i}^{+} = \int_0^1 \xi \vec{m}_a \Delta L_i d\xi \tag{16}$$

with $\vec{f}_a$ and $\vec{m}_a$ the distributed forces and moments. From Eqs (9)-(16), subscripts a, b or B referred to the development frame. Derivations $\dot{()}$ are made in the inertial frame.

The resulting nonlinear system of $18N+12$ equations consists in

- $12(N-1)$ equations associated to intermediate nodes:

  $\vec{f}_{u_i}^+ + \vec{f}_{u_{i+1}}^- = \vec{0}$; $\vec{f}_{\psi_i}^+ + \vec{f}_{\psi_{i+1}}^- = \vec{0}$;
  $\vec{f}_{F_i}^+ + \vec{f}_{F_{i+1}}^- = \vec{0}$; $\vec{f}_{M_i}^+ + \vec{f}_{M_{i+1}}^- = \vec{0}$

- 12 equations associated to the starting node:

  $\vec{f}_{u_1}^- - \hat{\vec{F}}_1 = \vec{0}$; $\vec{f}_{\psi_1}^- - \hat{\vec{M}}_1 = \vec{0}$;
  $\vec{f}_{F_1}^- - \hat{\vec{u}}_1 = \vec{0}$; $\vec{f}_{M_1}^- - \hat{\vec{\theta}}_1 = \vec{0}$

- 12 equations associated to the ending node:

  $\vec{f}_{u_N}^+ + \hat{\vec{F}}_{N+1} = \vec{0}$; $\vec{f}_{\psi_1}^- + \hat{\vec{M}}_1 = \vec{0}$;
  $\vec{f}_{F_1}^- + \hat{\vec{u}}_1 = \vec{0}$; $\vec{f}_{M_1}^- + \hat{\vec{\theta}}_1 = \vec{0}$

- $6N$ equations associated to the elements:

$$\vec{f}_{P_i} = \vec{0}; \qquad \vec{f}_{H_i} = \vec{0}$$

The corresponding $18N+12$ unknowns are $\vec{u}_i$, $\vec{\theta}_i$, $\vec{F}_i$, $\vec{M}_i$ for each node and $\vec{P}_i$ and $\vec{H}_i$ for each element. Boundary conditions are prescribed to boundary nodes, either in displacement/rotation or in force/moment.

This formulation is so far purely structural. The aerodynamic part of the reduced order model will thus be injected into it throughout distributed forces and moment $\vec{f}_a$ and $\vec{m}_a$.

2.3 Finite state induced flow model

As required by the typical reduced frequencies of VFA, a two-dimensional unsteady aerodynamic model must be used [16]. Because of the low Mach number and the relatively high Reynolds number (order of magnitude of 10^6) the choice fell on inviscid potential flow theories. Many of them rely on Wagner formulation in time domain [17] and Theodorsen theory [18] in frequency domain. The latter is suitable for computing flutter speed but implies the use of iterative loop like the so called *p-k method*. Indeed, aerodynamic loads depends on reduced frequency through Theodorsen function which, in is turn, is a function of velocity. To compel with computation needs, a more suitable type of method has been developed derived from the latter namely finite state approximations [19]. Instead of modelling shed wake effect with Theodorsen function, finite state approximation computes it with a number N_S of states resolved from a set of N_S Ordinary Differential Equations (ODE) which could be solved at the same time as the non linear system of the beam formulation. The resultant equations gives convergence to both Theodorsen and Wagner functions.

A widely used finite state approximation for VFA or rotor blade aeroelasticity is the method developed by Peters et al. [6]. This formulation is implemented in our toolbox with the following aerodynamic loads:

$$\begin{aligned} L &= \pi\rho b^2 \left(\ddot{h} + U\dot{\alpha} - ba\ddot{\alpha}\right) \\ &\quad + 2\pi\rho U b \left[\dot{h} + U\alpha + b\left(\frac{1}{2} - a\right)\dot{\alpha} - \lambda_0\right] \end{aligned} \tag{17}$$

$$\begin{aligned} M &= b\left(\frac{1}{2} + a\right) L \\ &\quad - \pi\rho b^3 \left[\frac{1}{2}\ddot{h} + u\dot{\alpha} + b\left(\frac{1}{8} - \frac{a}{2}\right)\ddot{\alpha}\right] \end{aligned} \tag{18}$$

with L the linear lift, M the linear moment around a reference point F, ρ the air density and U the flow velocity. The semi-chord b, the height h, AoA α and the distance a between the point F and the semi-chord are detailed in figure 3.

The induced-flow velocity λ_0 is approximated using N_S induced-flow states $\lambda_1, \lambda_2, \ldots, \lambda_{N_S}$ by:

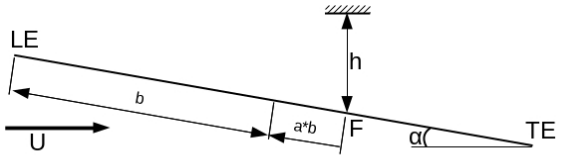

Figure 3: Airfoil parameters

$$\lambda_0 \approx \frac{1}{2}\sum_{n=1}^{N_S} b_n \lambda_n$$

where the b_n are found in [20] by the least-squares method. The induced-flow dynamics then are derived from the assumption that the shed vorticity stay in the plane of the airfoil and travel downstream with the same velocity as the flow. $\vec{\lambda}$ is a column matrix containing the values of λ_n determined using a set of N_S first-order ODEs [20]:

$$\vec{\vec{A}}\dot{\vec{\lambda}} + \frac{U}{b}\vec{\lambda} = \left[\ddot{h} + U\dot{\theta} + b\left(\frac{1}{2} - a\right)\ddot{\theta}\right]\vec{c} \tag{19}$$

Matrix $\vec{\vec{A}}$ is defined by:

$$\vec{\vec{A}} = \vec{\vec{D}} + \vec{d}\vec{b}^T + \vec{c}\vec{d}^T + \frac{1}{2}\vec{c}\vec{b}^T \tag{20}$$

where

$$D_{nm} = \begin{cases} \frac{1}{2n} & n = m+1 \\ -\frac{1}{2n} & n = m-1 \\ 0 & n \neq m \pm 1 \end{cases} \tag{21}$$

$$b_n = \begin{cases} (-1)^{n-1} \frac{(N_S+n-1)!}{(N_S-n-1)!} \frac{1}{(n!)^2} & n \neq N_S \\ (-1)^{n-1} & n = N_S \end{cases} \tag{22}$$

$$d_n = \begin{cases} \frac{1}{2} & n = 1 \\ 0 & n \neq 1 \end{cases} \tag{23}$$

$$c_n = \frac{2}{n} \tag{24}$$

The aerodynamic model adds N_S equations for each member, the coupled aeroelastic system contains $(18+N_S)N+12$ equations and the same number of unknowns, providing that structural unknowns are completed with $N \times N_S$ induced-flow states λ_{n_i}. Hereinafter the system of equations will be written as:

$$\mathscr{F}(\vec{X}, \dot{\vec{X}}) = \vec{0} \tag{25}$$

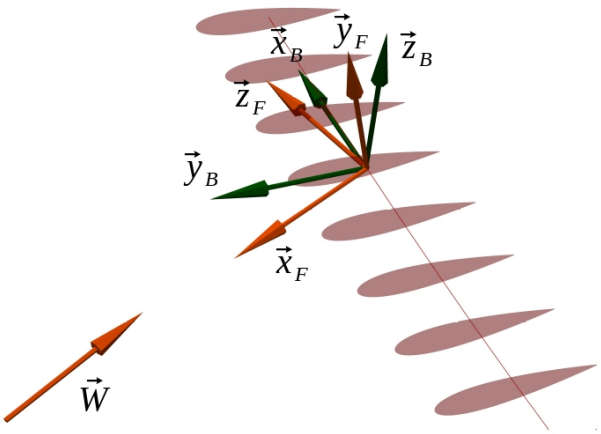

Figure 4: Flow frame definition

2.4 Fluid/structure integration

Aerodynamic loads directions are defined relatively to the orientation of the wind $\vec{W}$. According to that point, we defined a forth type of frame, namely a flow frame $(\vec{x}_F, \vec{y}_F, \vec{z}_F)$ consistent with two-dimensional aerodynamic conventions. This orthonormal triad of unit vector is defined as follow (figure 4).

$$\vec{x}_F = -\vec{W}$$

The lift forces directed by $\vec{y}_F$ is normal to the wind and to the deformed wing surface:

$$\vec{y}_F = \frac{\vec{x}_B \wedge \vec{x}_F}{\|\vec{x}_B \wedge \vec{x}_F\|}$$

The aerodynamic moment direction $\vec{z}_F$ complements the orthonormal triad of unit vectors:

$$\vec{z}_F = \vec{x}_F \wedge \vec{y}_F$$

Using these definitions, the tight coupling requires to link aerodynamic and structural unknowns. We defined, under the assumption that wind direction and velocity are constant in time or quasi-steady:

- α the local AoA, $\alpha \in]-90°, 90°[$

$$\alpha = \arcsin\left(\vec{y}_B . \vec{y}_F\right) \tag{26}$$

- β the local yaw angle, $\beta \in]-90°, 90°[$

$$\beta = \arcsin\left(\vec{y}_B . \vec{z}_F\right) \tag{27}$$

- U the local flow velocity

$$U = U_\infty \cos\beta \tag{28}$$

with U_∞ the upstream flow velocity.

- The time derivatives $\dot{\alpha}$, $\ddot{\alpha}$, $\dot{h}$, $\ddot{h}$:

$$\dot{\alpha} = \vec{\Omega}_a . \vec{z}_F = \left(\vec{\vec{C}}^T \vec{\vec{C}}^{ab} \vec{\Omega}_B\right) . \vec{z}_F \tag{29}$$

$$\ddot{\alpha} \simeq \dot{\vec{\Omega}}_a . \vec{z}_F \tag{30}$$

$$\dot{h} = -\vec{V}_a . \vec{z}_F = -\left(\vec{\vec{C}}^T \vec{\vec{C}}^{ab} \vec{V}_B\right) . \vec{y}_F \tag{31}$$

$$\ddot{h} \simeq -\dot{\vec{V}}_a . \vec{z}_F \tag{32}$$

Then, unsteady aerodynamic loads, considered constant within each element, are injected in distributed beam loads as:

$$\vec{f}_a = L\vec{y}_F \tag{33}$$
$$\vec{m}_a = M\vec{z}_F \tag{34}$$

using Eqs (26)-(32) to substitute aerodynamic unknowns with structural ones.

2.5 Flutter speed computation

The formulation described in section 2 permits different applications

- Study nonlinear transient dynamic behavior using a time marching scheme;
- Study nonlinear steady-state dynamic behavior by neglecting all the time derivatives;
- Realise an eigenvalue analysis of small motion about a steady-state by linearising about it.

One of the main advantage of the tight coupling is the ability to compute aeroelastic modes. In that case, the solution vector is written:

$$\vec{X}(t) = \overline{\vec{X}} + \breve{\vec{X}}(t) \tag{35}$$

with $\overline{\vec{X}}$ the steady-state solution and $\breve{\vec{X}}(t) \ll \overline{\vec{X}}$. As a results in Eq. (25) and performing a Taylor expansion, the system becomes, keeping first order terms:

$$\mathscr{F}(\overline{\vec{X}} + \breve{\vec{X}}(t), \breve{\dot{\vec{X}}}) = \mathscr{F}(\overline{\vec{X}}, \vec{0}) + \frac{\partial \mathscr{F}}{\partial \breve{\vec{X}}} \breve{\vec{X}} + \frac{\partial \mathscr{F}}{\partial \breve{\dot{\vec{X}}}} \breve{\dot{\vec{X}}} = \vec{0} \tag{36}$$

assuming that $\mathscr{F}(\overline{\vec{X}}, \vec{0}) = \vec{0}$ (steady-state solution) Eq. (36) becomes:

$$\frac{\partial \mathscr{F}}{\partial \breve{\vec{X}}} \breve{\vec{X}} + \frac{\partial \mathscr{F}}{\partial \breve{\dot{\vec{X}}}} \breve{\dot{\vec{X}}} = \vec{0}$$

For an eigenvalue analysis, we assume that:

$$\breve{\vec{X}}(t) = \tilde{X}_0 e^{\nu t} \tag{37}$$

It gives us the following Generalised Eigenvalue Problem (GEP):

$$\left(\frac{\partial \mathscr{F}}{\partial \tilde{\vec{X}}} + \nu \frac{\partial \mathscr{F}}{\partial \dot{\tilde{\vec{X}}}}\right) \tilde{X}_0 = \vec{0} \tag{38}$$

By analogy with classical dynamic resolutions, $\frac{\partial \mathscr{F}}{\partial \tilde{\vec{X}}}$ refers to a stiffness matrix $\vec{\vec{K}}$ and $\frac{\partial \mathscr{F}}{\partial \dot{\tilde{\vec{X}}}}$ to a mass matrix $\vec{\vec{M}}$. They must not be confused with stiffness matrix $\vec{\vec{S}}$ and mass matrix $\vec{\vec{I}}$ defined in section 2.2.

Because of the use of Lagrange multiplier inherent to the geometrically exact beam theory and the addition of induced-flow ODE, this GEP is real and non-symmetric. Neither stiffness nor mass matrix is symmetric positive semi-definite, thus our GEP requires a direct transformation into a Standard Eigenvalue Problem (SEP) :

$$\vec{\vec{K}}^{-1}\vec{\vec{M}}\tilde{X}_0 = -\frac{1}{\nu}\tilde{X}_0 \tag{39}$$

Direct inversion of $\vec{\vec{K}}$ is avoided using the resolution of a linear system :

$$\vec{\vec{K}}\vec{V} = \vec{Z} \tag{40}$$

with $\vec{V} = \vec{\vec{K}}^{-1}\vec{\vec{M}}\tilde{X}_0$ and $\vec{Z} = \vec{\vec{M}}\tilde{X}_0$

Because we only need the computation of a few eigenvalues corresponding to the lower frequencies aeroelastic modes, the SEP is resolved using the Implicitly Restarted Arnoldi Method (IRAM) implemented into open source ARPACK program (ARnoldi PACKage) [21]. Matrices are stored in coordinate list sparse format (COO). In order to propose a fully open source solution, the sparse direct linear solver required by Eq. (40) is MUMPS (MUltifrontal Massively Parallel sparse direct Solver) [22], replacing HSL (Harwell Subroutine Library) MA28 library initially used in GEBT program [10]. A significant proportion of computation time comes from the resolution of Eq. (40), then special attention is devoted to optimise the configuration of MUMPS. Before the resolution of the SEP, rows and columns are reordered using software package Scotch and are scaled. The strategy followed in our toolbox consists in relying on well optimised and maintained Fortran open source libraries.

Induced-flow ODEs [6] add purely real eigenvalues to the initial structural problem with relatively small magnitude which are not associated with aeroelastic modes. Because the SEP resolved is the invert of the initial GEP and to avoid induced-flow eigenvalues, modes of interest correspond to the eigenvalues with the largest imaginary part. Then, replacing complex eigenvalue ν with $a+ib$ in Eq. (37), unstable modes are identified when a positive value of a is found. Considering that, a Python routine is used to find the lowest flow velocity associated with an unstable mode corresponding to the flutter speed.

3 VALIDATION TEST CASES

Besides tests conducted to validate the homogenisation step [15, 23], present section intends to prove both accuracy and speed of our toolbox using widely used aeroelastic test cases, namely the Goland wing [24] and the Patil wing [25]. The first is universally used among literature and the second is more appropriate to our program because of its high-aspect-ratio. Unfortunately, both of them concern isotropic wing since there is no common anisotropic test case among the literature.

Concerning the speed evaluation, tests are conducted on a laptop PC (CPU : Intel® Core™ i5-4210H; RAM : 8GO; OS : Ubuntu 17.10) and compare the freely available toolbox Aeroflex used with Matlab R2017b with the present program compiled using GFortran 7.2 runing on a single core.

The Python routine uses a dichotomy to find the lowest flow velocity associated with an unstable mode. According to data from Table 1 and considering an isotropic case, wing characteristics can be directly inserted into mass and flexibility matrix skipping the homogenisation step, the reference point F is taken at the elastic center :

$$\vec{\vec{S}}^{-1} = \begin{bmatrix} 0 & 0 & 0 & 0 & 0 & 0 \\ 0 & 0 & 0 & 0 & 0 & 0 \\ 0 & 0 & 0 & 0 & 0 & 0 \\ 0 & 0 & 0 & 1/GJ & 0 & 0 \\ 0 & 0 & 0 & 0 & 1/EI_{G2} & 0 \\ 0 & 0 & 0 & 0 & 0 & 1/EI_{G3} \end{bmatrix}$$

$$\vec{\vec{I}} = \begin{bmatrix} \mu & 0 & 0 & 0 & 0 & \mu v \\ 0 & \mu & 0 & 0 & 0 & 0 \\ 0 & 0 & \mu & -\mu v & 0 & 0 \\ 0 & 0 & -\mu v & i_{11} & 0 & 0 \\ 0 & 0 & 0 & 0 & 0 & 0 \\ \mu v & 0 & 0 & 0 & 0 & i_{11} \end{bmatrix}$$

First of all, a convergence of the undeformed Goland wing flutter speed relatively to N and N_s parameters are realised (figure 5). It appears that a reasonable value for N start from 6, parameter N_S shows good results from 4. Because of the factorial entering into definition of $\vec{\vec{A}}$ (Eq. (20)) and $\vec{b}$ (Eq. (22)), N_s is limited to 8 in order to avoid roundoff errors and ill-conditioned matrices.

At the same time, computation speed is assessed on figure (6). The search interval of the dichotomy routine is set between 10 and 400 m/s with a precision of 10^{-2} m/s. The result is found in about 15 iterations, each of them corresponding to the resolution of a particular GEP. According to figure 6, computation time seems to be in the order of $O(N)$, paving the way for complex airframe simulations.

By comparison, Aeroflex with $N_s = 4$ takes $4.8\,s$ if $N = 2$, $98.8\,s$ if $N = 10$ and $751.1\,s$ if $N = 20$. Several reasons could explain the big gap between both program,

Table 1: Characteristics of Goland and Patil wings

			Goland [24]	Patil [25]
Semi-span	L	m	6.096	16
Chord	$2b$	m	1.8288	1
Mass per unit length	μ	kg/m	35.71	0.75
Elastic axis (from leading edge)		% chord	33	50
Center of gravity (from leading edge)		% chord	43	50
Distance between CG and EA	v	m	0.18288	0
Bending stiffness (span-wise)	EI_{G2}	N.m^2	9.77×10^6	2.10^4
Bending stiffness (chord-wise)	EI_{G3}	N.m^2	/	4.10^6
Torsional stiffness	GJ	N.m^2	0.99×10^6	1.10^4
Mass moment of inertia around e.a.	i_{11}	kg.m	8.64	0.10

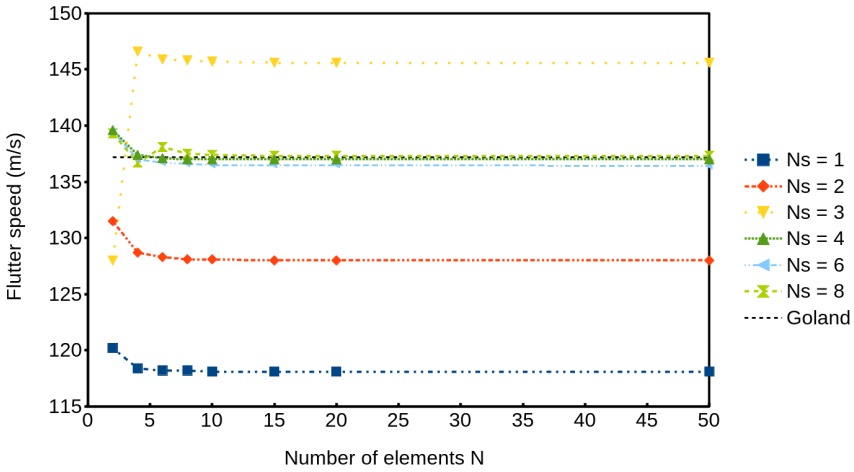

Figure 5: Convergence tests for N and N_s parameters

among them the use of sparse matrix versus dense matrix or the use of compiled language (Fortran) versus interpreted language (Matlab).

Then the flutter speed and frequency are computed at sea level ($\rho = 1.225 kg.m^{-3}$) and at 20000 ft ($\rho = 0.6526 kg.m^{-3}$) using $N = 10$ elements and $N_S = 6$ induced-flow states and compared to literature. Results are presented in Table 2.

Results show a good agreement with other strip theory reduced order models whereas UVLM based models predict a higher critical speed because of three-dimensional effects. A more appropriate test case is the Patil high-aspect-ratio wing whose characteristics are detailed in Table 1. Besides undeformed wing flutter speed assessment, flutter speed is also calculated about the wing deformed by the lift compensating its own weight (aircraft AoA is iteratively modified to compensate the weight at flutter speed). Both simulations are made using $N = 10$ and $N_S = 6$ and demonstrate also a good agreement (Table 3). Computation time with a search interval of 1 to 100 m/s and a precision of 10^{-2} m/s is 0.35 s for the undeformed wing and 3.22 s for the deformed wing (longer because of the iterative aircraft AoA adjustment).

4 CONCLUSION

Design challenges induced by HAPS in terms of aeroelastic performances show the need for an accurate reduced order model able to simulate nonlinear behavior of an anisotropic high-aspect-ratio wing. The present work presents a solution based of the geometrically exact beam theory coupled with a two-dimensional unsteady finite state aerodynamic model implemented into an open source solver. Accuracy of flutter speed computation on both undeformed and deformed wing has been demonstrated using common aeroelastic test cases. Aeroelastic tailoring, a composite material technology designed to further flutter speed without being detrimental to mass balance, requires the use of an optimisation loop for which flutter speed computation time is a key feature. Tests conducted using different parameters show that the present program fully meets this requirement, thanks to the use of optimised Fortran open source computation libraries.

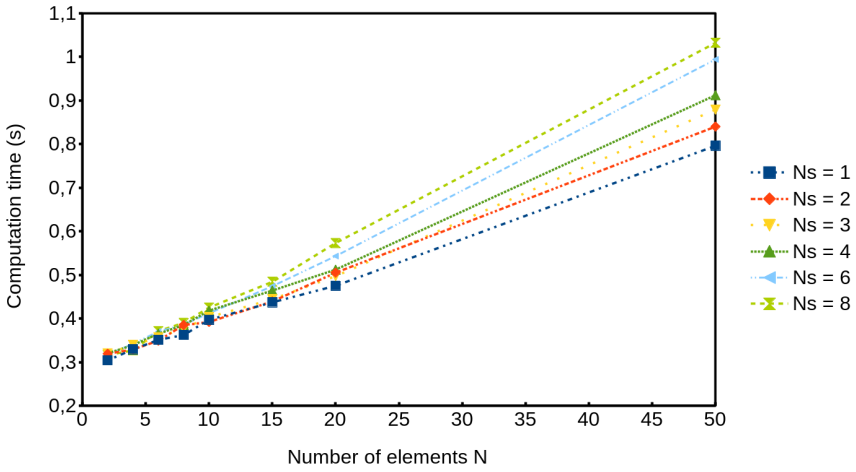

Figure 6: Goland flutter speed computation time (dichotomy interval:$[10,400]$ m/s, precision: 10^{-2} m/s)

Table 2: Goland wing flutter speed and frequency

program	sea level		20000 ft	
	speed (m/s)	frequency (rad/s)	speed (m/s)	frequency (rad/s)
present ($N = 10$; $N_S = 6$)	136.5	70.3	174.9	69.0
Goland [26]	137.2	70.7	-	-
NATASHA[25]	135.6	70.2	-	-
UM/NAST[27]	136.2	70.2	174.9	68.1
SHARP[3]	165	69	-	-
Aeroflex[7]	137.0	70.8	177.0	69.2

REFERENCES

[1] Thomas E. NOLL, John M. BROWN, Marla E. PEREZ-DAVIS, Stephen D. ISHMAEL, Geary C. TIFFANY et Matthew GAIER : Investigation of the Helios prototype aircraft mishap. *NASA Report*, 9, 2004. 1

[2] Zhicun WANG, P. C. CHEN, D. D. LIU et D. T. MOOK : Nonlinear-aerodynamics/nonlinear-structure interaction methodology for a high-altitude long-endurance wing. *Journal of Aircraft*, 47(2):556–566, 2010. 1

[3] Joseba MURUA, Rafael PALACIOS et J. Michael R. GRAHAM : Assessment of wake-tail interference effects on the dynamics of flexible aircraft. *AIAA journal*, 50(7):1575–1585, 2012. 1, 2

[4] Mark DRELA : Integrated simulation model for preliminary aerodynamic, structural, and control-law design of aircraft. *AIAA Paper*, 99:1394, 1999. 1

[5] Christopher M. SHEARER et Carlos ES CESNIK : Nonlinear flight dynamics of very flexible aircraft. *Journal of Aircraft*, 44(5):1528–1545, 2007. 1

[6] David A. PETERS, Swaminathan KARUNAMOORTHY et Wen-Ming CAO : Finite state induced flow models. I-Two-dimensional thin airfoil. *Journal of Aircraft*, 32(2):313–322, 1995. 1, 2.3, 2.5

[7] Flavio Luiz Cardoso RIBEIRO, Pedro PAGLIONE, Roberto Gil Annes da SILVA et Marcelo Santiago de SOUSA : Aeroflex: a toolbox for studying the flight dynamics of highly flexible airplanes. 2012. 1, 2, 3

[8] C.-S. CHANG, Dewey H. HODGES et Mayuresh J. PATIL : Flight dynamics of highly flexible aircraft. *Journal of Aircraft*, 45(2):538–545, 2008. 1

[9] Jason M. JONKMAN et M. L. BUHL JR : FAST User s Guide, National Renewable Energy Laboratory. *No. NREL/EL-500-38230, Golden, CO*, 2005. 2

[10] Wenbin YU et Maxwell BLAIR : GEBT: A general-purpose nonlinear analysis tool for composite beams. *Composite Structures*, 94(9):2677–2689, 2012. 2.2, 2.2, 2.5

[11] Dewey H. HODGES : A mixed variational formulation based on exact intrinsic equations for dynamics

Table 3: Patil wing flutter speed and frequency

program	Undeformed wing		Deformed wing	
	speed (m/s)	frequency (rad/s)	speed (m/s)	frequency (rad/s)
present ($N = 10$; $N_S = 6$)	32.2	22.6	23.3	11.9
NATASHA[25]	32.2	22.6	-	-
UM/NAST[28]	32.2	22.6	23.2	10.3
Aeroflex[7]	32.6	22.3	23.4	12.2

of moving beams. *International journal of solids and structures*, 26(11):1253–1273, 1990. 2.2, 2.2

[12] Dewey H. HODGES, Xiaoyang SHANG et Carlos ES CESNIK : Finite element solution of nonlinear intrinsic equations for curved composite beams. *Journal of the American helicopter society*, 41(4):313–321, 1996. 2.2

[13] Carlos ES CESNIK et Dewey H. HODGES : VABS: a new concept for composite rotor blade cross-sectional modeling. *Journal of the American Helicopter Society*, 42(1):27–38, 1997. 2.2

[14] G. DHONDT et K. WITTIG : Calculix: a free software three-dimensional structural finite Element Program. *MTU Aero Engines GmbH, Munich, Germany*, 1998. 2.2

[15] Bertrand KIRSCH, Olivier MONTAGNIER, Emmanuel BÉNARD et Thierry M. FAURE : Dynamic aeroelastic simulation of composite wing for HALE UAV application. *European Conference for Aeronautics and Space Sciences*, 2017. 2.2, 3

[16] H. HADDADPOUR et R. D. FIROUZ-ABADI : Evaluation of quasi-steady aerodynamic modeling for flutter prediction of aircraft wings in incompressible flow. *Thin-walled structures*, 44(9):931–936, 2006. 2.3

[17] Herbert WAGNER : Über die Entstehung des dynamischen Auftriebes von Tragflügeln. *ZAMM-Journal of Applied Mathematics and Mechanics/Zeitschrift für Angewandte Mathematik und Mechanik*, 5(1):17–35, 1925. 2.3

[18] Theodore THEODORSEN : General theory of aerodynamic instability and the mechanism of flutter. *NACA Technical Report*, (NACA-TR-496), 1935. 2.3

[19] David A. PETERS : Two-dimensional incompressible unsteady airfoil theory—an overview. *Journal of Fluids and Structures*, 24(3):295–312, 2008. 2.3

[20] Dewey H. HODGES et G. Alvin PIERCE : *Introduction to structural dynamics and aeroelasticity*, volume 15. cambridge university press, 2011. 2.3

[21] R. B. LEHOUCQ, D. C. SORENSEN et C. YANG : ARPACK Users' Guide: Solution of Large Scale Eigenvalue Problems with Implicitly Restarted Arnoldi Methods. *Software Environ. Tools*, 6, 1997. 2.5

[22] Patrick R. AMESTOY, Iain S. DUFF, Jean-Yves L'EXCELLENT et Jacko KOSTER : A fully asynchronous multifrontal solver using distributed dynamic scheduling. *SIAM Journal on Matrix Analysis and Applications*, 23(1):15–41, 2001. 2.5

[23] Bertrand KIRSCH, Olivier MONTAGNIER, Emmanuel BÉNARD et Thierry FAURE : Contribution of composite anisotropy in HALE drones aeroelastic performances. *In Journées Nationales sur les Composites 2017*, 77455 Champs-sur-Marne, France, juin 2017. École des Ponts ParisTech (ENPC). 3

[24] Martin GOLAND : The flutter of a uniform cantilever wing. *Journal of Applied Mechanics-Transactions of the Asme*, 12(4):A197–A208, 1945. 3, 1

[25] Mayuresh J. PATIL : *Nonlinear aeroelastic analysis, flight dynamics, and control of a complete aircraft*. Thèse de doctorat, Citeseer, 1999. 3, 1, 2, 3

[26] Martin GOLAND et Y. L. LUKE : The flutter of a uniform wing with tip weights. *Journal of Applied Mechanics*, 15(1):13–20, 1948. 2

[27] Eric Lee BROWN : *Integrated strain actuation in aircraft with highly flexible composite wings*. Thèse de doctorat, Massachusetts Institute of Technology, 2003. 2

[28] Weihua SU : *Coupled nonlinear aeroelasticity and flight dynamics of fully flexible aircraft*. Thèse de doctorat, University of Michigan, 2008. 3